1854 *Inorg. Chem.* **2010**, *49*, 1854–1864
DOI: 10.1021/ic902220a

Inorganic Chemistry
Article

Binding of Nitric Oxide to a Synthetic Model of Iron-Containing Nitrile Hydratase (Fe-NHase) and Its Photorelease: Relevance to Photoregulation of Fe-NHase by NO

Michael J. Rose, Nolan M. Betterley, Allen G. Oliver, and Pradip K. Mascharak*

Department of Chemistry and Biochemistry, University of California, 1156 High Street, Santa Cruz, California 95064

Received November 10, 2009

The activity of the non-heme iron enzyme nitrile hydratase (Fe-NHase) is modulated by nitric oxide (NO). The inactive (dark form) NO-bound enzyme is activated when exposed to light via the release of NO from the iron center. In order to determine whether oxygenation of active site Fe-bound Cys-S centers are involved in this process of NO regulation, a model complex $(Et_4N)[(Cl_2PhPepS)Fe(NO)(DMAP)]$ (**8**) has been synthesized and structurally characterized. Complex **8** does not exhibit any NO photolability. However, following oxygenation of the Fe-bound thiolato-S centers to sulfinates (with the aid of oxaziridine), the resulting complex $(Et_4N)[(Cl_2PhPep\{SO_2\}_2)$-$Fe(NO)(DMAP)]$ (**9**) releases NO readily upon illumination with visible light. Spectroscopic properties of **8** and **9** confirm that these species do mimic the active site of Fe-NHase closely, and the results indicate that NO photolability is related to S-oxygenation. Results of density functional theory and time-dependent DFT studies on both **8** and **9** indicate that S-oxygenation weakens Fe−S bonding and that strong transitions near 470 nm transfer an electron from a carboxamido-N/sulfinato-SO_2 MO to a $d\pi$(Fe)-π^*(NO)/d_z2(Fe)-σ^*(NO) antibonding orbital in **9**. In case of **8**, strong S−Fe−NO bonding interactions prevent the release of NO upon illumination. Together, the results of this work strongly suggest that oxygenated Cys-S centers play an important role in the process of NO regulation of Fe-NHases.

Introduction

The enzyme nitrile hydratase (NHase) plays an important role in the microbial assimilation of organic nitriles[1] and catalyzes the conversion of nitriles into corresponding amides.[2,3] The active site of the enzyme contains either a nonheme Fe(III) or a noncorrinoid Co(III) center bound to two carboxamido-N and three cysteine-S donors.[4,5] Two of the three cysteine-S ligands are post-translationally modified to a sulfenato (−SO) and a sulfinato ($-SO_2$) moiety.[6] In addition to the unusual donors around the metal center, the iron-conaining NHases (Fe-NHase) can contain a Fe-bound nitric oxide (NO) molecule in the coordination sphere of the metal.[7,8] This form, often referred to as the "dark form", has been purified (Fe-NHase from *Rhodococcus* species R312 or N771) and characterized structurally by Endo and co-workers.[8] The dark form of Fe-NHase is catalytically inactive. Exposure to light causes rapid loss of NO, and the subsequent binding of water activates the enzyme for catalysis.[9] Recently, the X-ray structure of Fe-NHase by Qian and co-workers revealed the presence of two sulfinato ($-SO_2$) groups around the iron center.[10]

*Corresponding author. Telephone: (831) 459-4251. Fax: (831) 459-2935. E-mail: pradip@chemistry.ucsc.edu.

(1) Endo, I.; Nojiri, M.; Tsujimura, M.; Nakasako, M.; Nagashima, S.; Yohda, M.; Odaka, M. *J. Inorg. Biochem.* **2001**, *83*, 247–253.
(2) (a) Kobayashi, M.; Shimizu, S. *Curr. Opin. Chem. Biol.* **2000**, *4*, 95–102. (b) Endo, I.; Odaka, M.; Yohda, M. *Trends Biotechnol.* **1999**, *17*, 244–248.
(3) (a) Harrop, T. C.; Mascharak, P. K. *Acc. Chem. Res.* **2004**, *37*, 253–260. (b) Kovacs, J. A. *Chem. Rev.* **2004**, *104*, 825–848. (c) Mascharak, P. K. *Coord. Chem. Rev.* **2002**, *225*, 201–214.
(4) Huang, W. J.; Jia, J.; Cummings, J.; Nelson, M.; Schneider, G.; Lindqvist, Y. *Structure* **1997**, *5*, 691–699.
(5) Miyanga, A.; Fushinobu, S.; Ito, K.; Wakagi, T. *Biochem. Biophys. Res. Commun.* **2001**, *288*, 1169–1174.
(6) Tsujimura, M.; Dohmae, N.; Odaka, M.; Chijimatsu, M.; Takio, K.; Yohda, M.; Hoshino, M.; Nagashima, S.; Endo, I. *J. Biol. Chem.* **1997**, *272*, 29454–29459.
(7) (a) Endo, I.; Nojiri, M.; Tsujimura, M.; Nakasako, M.; Nagashima, S.; Yohda, M.; Odaka, M. *J. Inorg. Biochem.* **2001**, *83*, 247–253. (b) Nagamune, T.; Kurata, H.; Hirata, M.; Honda, J.; Hirata, A.; Endo, I. *Photochem. Photobiol.* **1990**, *51*, 87–90. (c) Nagamune, T.; Kurata, H.; Hirata, M.; Honda, J.; Koike, H.; Ikeuchi, M.; Inoue, Y.; Hirata, A.; Endo, I. *Biochem. Biophys. Res. Commun.* **1990**, *168*, 437–442.
(8) Nagashima, S.; Nakasako, M.; Dohmae, N.; Tsujimura, M.; Takio, K.; Odaka, M.; Yohda, M.; Kamiya, N.; Endo, I. *Nat. Struct. Biol.* **1998**, *5*, 347–351.
(9) (a) Odaka, M.; Fujiii, K.; Hoshino, M.; Noguchi, T.; Tsujimura, M.; Nagashima, S.; Yohda, M.; Nagamune, T.; Inoue, Y.; Endo, I. *J. Am. Chem. Soc.* **1997**, *119*, 3785–3791. (b) Noguchi, T.; Hoshino, M.; Tsujimura, M.; Odaka, M.; Inoue, Y.; Endo, I. *Biochemistry* **1996**, *35*, 16777–16781. (c) Noguchi, T.; Honda, J.; Nagamune, T.; Sasabe, H.; Inoue, Y.; Endo, I. *FEBS Lett.* **1995**, *358*, 9–12.
(10) Song, L.; Wang, M. Z.; Shi, J. J.; Xue, Z. Q.; Wang, M. X.; Qian, S. J. *Biochem. Biophys. Res. Commun.* **2007**, *362*, 319–324.

Published on Web 01/12/2010

The exact role of the S-oxygenated donors in NO photoregulation of Fe-NHase, however, remains elusive.

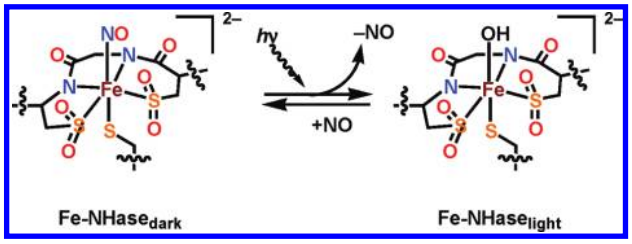

Recent modeling approaches have provided insight into the structure−function relationship of the donor atoms in NHases.[3] At least three different groups have synthesized models of the NO-bound active site.[11−13] Despite such success, none of these models of the dark form of Fe-NHase exhibits NO photolability. Close examination of these models of NO-bound Fe-NHase reveals that in no case have all of the donor centers been assembled around the Fe center. For example, in all cases both thiolato-S donors and NO are included in the coordination sphere of iron, but no sulfinato ($-SO_2$) group is present.[11−13] On the other hand, model complexes reported previously by us[14−16] as well as Artaud and co-workers[17,18] contain coordinated sulfinato groups (in different binding modes), but the absence of bound NO precluded studies on NO photolability. In the present work, we have used a model of the Fe-NHase active site derived from a designed N2S2 ligand namely, 4,5-dichloro-*N*,*N*′-phenylenebis(*o*-mercaptobenzamide) ($Cl_2PhPepSH_4$; where H = dissociable amide and thiol Hs), to determine the role of S-oxygenation in the process of NO photorelease from the metal site. By using a new S-oxygenation method, we have examined the effect of thiolato-S oxygenation (to $-SO_2$) on NO binding to the Fe(III) species $(Et_4N)[(Cl_2PhPepS)Fe(DMAP)]$ (**7**) and on photorelease of NO from $(Et_4N)[(Cl_2PhPepS)Fe(NO)(DMAP)]$ (**8**) and $(Et_4N)[(Cl_2PhPep\{SO_2\}_2)Fe(NO)(DMAP)]$ (**9**). We report herein that, although **8** (a close structural mimic of the active site of NO-bound Fe-NHase) does not exhibit any NO photolability, S-oxygenation serves as a "chemical switch" to allow NO photorelease from **9**. The results of density functional theory (DFT) calculations are also presented to provide insight into the origin of this photolability.

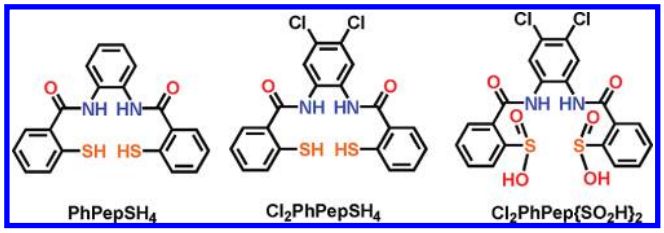

Experimental Section

General Procedures. All reagents including *N*,*N*-dimethylaminopyridine (DMAP), 4,5-dichlorodiaminobenzene, and thiosalicylic acid were purchased from Aldrich Chemical Co. and used without further purification. All solvents were obtained from Fisher Scientific and distilled from standard drying agents as follows: diethyl ether (Et_2O) and tetrahydrofuran (THF) from Na, acetonitrile (MeCN) and dichloromethane (CH_2Cl_2) from calcium hydride (CaH_2), dimethylformamide (DMF) from barium oxide (BaO), and methanol (MeOH) and ethanol (EtOH) from magnesium iodide (MgI_2). Standard Schlenk technique was used, and solutions were degassed by the freeze−pump−thaw method. NO gas was supplied by Spectra Gases Inc. and purified as previously described.[19] The starting material 2,2′-dithiosalicyl chloride and the ligand $PhPepSH_4$ were synthesized as previously described,[20] while the ligand $Cl_2PhPepSH_4$ was synthesized according to a slightly modified procedure (see Ligand Synthesis).

Ligand Synthesis. **$Cl_2PhPepS_2$.** A batch of 2,2′-dithiosalicyl chloride (2.00 g, 5.83 mmol) was dissolved in 20 mL of CH_2Cl_2 and filtered through a cintered glass frit to remove trace amounts of the acid. Separately, a mixture of 4,5-dichloro-*o*-phenylenediamine (1.03 g, 5.83 mmol) and excess triethylamine (Et_3N, 1.76 g, 17.5 mmol) was prepared in 25 mL of CH_2Cl_2. The diamine/Et_3N mixture was quickly added to a stirred solution of the acid chloride. The resulting solution was stirred for 12 h, after which the solvent was removed in vacuo. The brown residue was treated with 5 mL of MeOH, and the resulting slurry stirred for 20 min. This beige solid was collected by filtration and washed with 20 mL of both cold MeOH and dry Et_2O. The yield of the disulfide macrocycle $Cl_2PhPepS_2$ was 60% (1.55 g). Selected IR bands (potassium bromide, KBr matrix, cm^{-1}): 3 430 (s, ν_{NH}), 1 665 (vs, ν_{CO}), 1 586 (m), 1 490 (vs), 1 374 (m), 1 134 (s), 1 037 (s), 904 (s), 743 (m), 476 (s).

$Cl_2PhPepSH_4$. A batch of $Cl_2PhPepS_2$ (1.55 g, 3.46 mmol) was mixed with 70 mL of distilled THF, and the resulting beige slurry was degassed by the freeze−pump−thaw technique. Upon warming to 0 °C, small portions of sodium borohydride ($NaBH_4$, 0.66 g, 17.3 mmol) were anaerobically added over several minutes, and the solution was periodically flushed with dry N_2 gas. The resulting dark-green slurry was then stirred overnight at room temperature. The next day the volume of the reaction mixture was reduced to 10 mL and diluted later with 10 mL of degassed H_2O. It was then neutralized with ~6 mL of 6 M acetic acid when the protonated ligand precipitated out as a beige solid. The ligand was collected by filtration and washed successively with 10 mL portions of H_2O, cold MeOH, and Et_2O. Yield: 1.09 g (70%). Selected IR bands (KBr matrix, cm^{-1}): 3 372 (w, ν_{NH}), 2 568 (w, ν_{SH}), 1 644 (vs, ν_{CO}), 1 588 (vs), 1 530 (vs),

(11) Schweitzer, D.; Ellison, J. J.; Shoner, S. C.; Lovell, S.; Kovacs, J. A. *J. Am. Chem. Soc.* **1998**, *120*, 10996–10997.
(12) Chatel, S.; Chauvin, A. S.; Tuchagues, J.-P.; Leduc, P.; Bill, E.; Chottard, J.-C.; Mansuy, D.; Artaud, I. *Inorg. Chim. Acta* **2002**, *336*, 19–28.
(13) (a) Grapperhaus, C. A.; Li, M.; Patra, A. K.; Poturovic, S.; Kozlowski, P. M.; Zgierski, M. Z.; Mashuta, M. S. *Inorg. Chem.* **2003**, *42*, 4382–4388. (b) Grapperhaus, C. A.; Patra, A. K.; Mashuta, M. S. *Inorg. Chem.* **2002**, *41*, 1039–1041.
(14) Noveron, J. C.; Olmstead, M. M.; Mascharak, P. K. *J. Am. Chem. Soc.* **2001**, *123*, 3247–3259.
(15) Tyler, L. A.; Noveron, J. C.; Olmstead, M. M.; Mascharak, P. K. *Inorg. Chem.* **1999**, *38*, 616–617.
(16) (a) Tyler, L. A.; Noveron, J. C.; Olmstead, M. M.; Mascharak, P. K. *Inorg. Chem.* **2003**, *42*, 5751–5761. (b) Tyler, L. A.; Noveron, J. C.; Olmstead, M. M.; Mascharak, P. K. *Inorg. Chem.* **2000**, *39*, 357–362.
(17) Galardon, E.; Giorgi, M.; Artuad, I. *Chem. Commun.* **2004**, 286–287.
(18) (a) Bourles, E.; de Sousa, R. A.; Galardon, E.; Giorgi, M.; Artaud, I. *Angew. Chem., Intl. Ed. Engl.* **2005**, *44*, 6162–6165. (b) Rat, M.; de Sousa, R. A.; Vaissermann, J.; Leduc, P.; Mansuy, D.; Artaud, I. *J. Inorg. Biochem.* **2001**, *84*, 207–213.
(19) Patra, A. K.; Rose, M. J.; Murphy, K. A.; Olmstead, M. M.; Mascharak, P. K. *Inorg. Chem.* **2004**, *43*, 4487–4495.
(20) (a) Harrop, T. C.; Olmstead, M. M.; Mascharak, P. K. *Inorg. Chem.* **2006**, *45*, 3424–3436. (b) Harrop, T. C.; Olmstead, M. M.; Mascharak, P. K. *J. Am. Chem. Soc.* **2004**, *126*, 14714–14715.

1 490 (vs), 1 452 (m), 1 369 (vs), 1 322 (vs), 1 262 (m), 1 137 (w), 879 (m), 742 (vs), 472 (w). ^{1}H NMR at 298 K in d^6-dimethyl sulfoxide (DMSO), (δ from tetramethlysilane, TMS): 10.19 (s 2H), 8.03 (s 2H), 7.76 (d 2H), 7.49 (d 2H), 7.36 (t 2H), 7.23 (t 2H), 5.35 (s 2H).

Syntheses of the Complexes. **($Et_4N)_2$[(Cl_2PhPepS)Fe(Cl)] (1).** A batch of $Cl_2PhPepSH_4$ (0.243 g, 0.54 mmol) was dissolved in 15 mL of degassed DMF at 0 °C and deprotonated with 0.058 g of NaH (2.43 mmol, added in small portions). Next, a solution of (Et_4N)[$FeCl_4$] (0.177 g, 0.53 mmol) in 5 mL of degassed DMF was added to it, and the resulting dark-red-brown solution was stirred overnight at room temperature. The next day, the solvent was removed in vacuo, and a solution of Et_4NCl (0.179 g, 1.08 mmol) in 30 mL of MeCN was added to it. After 30 min of stirring, the mixture was filtered to remove sodium chloride (NaCl), and the filtrate was concentrated to 5 mL. A batch of 15 mL of degassed Et_2O was added, and the mixture was stored at −20 °C. The brown microcrystalline product, obtained after 72 h, was collected by filtration and washed several times with small portions of Et_2O. Yield: 220 mg (56%). Anal. calcd for $C_{36}H_{50}Cl_3FeN_4O_2S_2$: C 54.23, H 6.33, N 7.03; found: C 54.38, H 6.23, N 6.95. Selected IR bands (KBr matrix, cm^{-1}): 2 980 (w), 1 585 (s, ν_{CO}), 1 569 (s), 1 533 (m), 1 478 (vs), 1 453 (vs), 1 391 (w), 1 311 (vs), 1 278 (m), 1 172 (w), 1 035 (w), 999, (w), 940 (w), 791 (w), 744 (m). UV/vis in MeCN, λ in nm (ε in M^{-1} cm^{-1}): 325 (19 070), 490 (2 800), 600 sh (2 280). Value of μ_{eff} (298 K, polycrystal): 3.81 μ_B.

($Et_4N)_2$[μ-S_2-{(Cl_2PhPepS)Fe(NO)}$_2$] (2). A degassed solution of **1** (0.070 g, 0.088 mmol) in 5 mL of MeCN was stirred vigorously at room temperature, and NO(g) was bubbled through it. A dark microcrystalline material appeared within 5 min. The reaction mixture was then stored at 4 °C for 30 min. The product was finally collected by filtration, washed several times with Et_2O, and dried in vacuo. Yield: 32 mg (60%). Anal. calcd for $C_{56}H_{60}Cl_4Fe_2N_8O_6S_4$: C 50.84, H 4.57, N 8.46; found: C 50.58, H 4.86, N 8.69. Selected IR bands (KBr matrix, cm^{-1}): 3 434 (m), 2 985 (w), 1 837 (vs, ν_{NO}), 1 585 (vs, ν_{CO}), 1 537 (vs), 1 453 (vs), 1 336 (vs), 1 182 (w), 1 111 (w), 1 084 (w), 950 (w), 915 (w), 787 (w), 750 (m), 677 (w), 574 (w). UV/vis in DMF, λ in nm (ε in M^{-1} cm^{-1}): 560 (5 000), 990 (3 030).

($Et_4N)_2$[(Cl_2PhPepS)Fe(NO)] (3). A solution of 5 mg (0.025 mmol) of (Et_4N)[p-ClC_6H_4S] in 2 mL of MeCN was slowly added to a solution of **1** (20 mg, 0.025 mmol) in 2 mL of MeCN. Next, 4 mL of degassed Et_2O was added, and the reaction mixture was cooled to −40 °C. One equiv of NO(g) (0.8 mL, 0.025 mmol) was then introduced into the head space via a gas-tight syringe, and the Schlenk flask was stored at −40 °C for 48 h. The dark-green microcrystals that separated were collected by filtration and dried in vacuo. Yield: 15 mg (80%). Anal. calcd for $C_{36}H_{50}Cl_2FeN_5O_3S_2$: C 54.61, H 6.37, N 8.85; found: C 54.85, H 6.54, N 8.79. Selected IR bands (KBr matrix, cm^{-1}): 1 631 (s ν_{NO}), 1 584 (vs ν_{CO}), 1 512 (s), 1 452 (vs), 1 332 (vs), 792 (w), 745 (w).

(Et_4N)[(Cl_2PhPepS)Fe(py)] (4). A solution of 8 mg (~2 equiv) of pyridine in 5 mL of MeCN was added to a solution of 0.100 g (0.120 mmol) of **1** in 5 mL of MeCN at room temperature. The color of the original brown-red solution rapidly changed to green. Next, a solution of 23 mg (0.120 mmol) of $AgBF_4$ in 5 mL of MeCN was added, and the mixture was stirred at room temperature for 10 min. It was then filtered (through a Celite pad) to remove the silver chloride (AgCl) precipitate, and the volume of the filtrate was reduced to ~3 mL. Following a thorough cooling of this solution at −40 °C, a batch of 15 mL of degassed Et_2O was added slowly when the dichroic red-green microcrystalline solid separated out. The product was collected by filtration and dried in vacuo. Yield: 55 mg (60%). Anal. calcd for $C_{33}H_{35}Cl_2FeN_4O_2S_2$: C 55.78, H 4.97, N 7.88; found: C 55.59, H 5.24, N 7.85. IR bands (KBr matrix, cm^{-1}): 1 591 (s, ν_{CO}), 1 455 (s), 1 310 (m), 1 261 (s), 941 (w), 800 (s), 746 (w), 696 (w). UV/vis in MeCN, λ in nm (ε in M^{-1} cm^{-1}): 320 (8 230), 610 (1 650).

(Et_4N)[(Cl_2PhPepS)Fe(1-Me-Im)] (**5**) and (Et_4N)[(Cl_2PhPepS)Fe(4-NH_2-py)] (**6**) were synthesized by following a similar procedure.

(Et_4N)[(Cl_2PhPepS)Fe(DMAP)] (7). A solution of 18 mg (0.15 mmol) of *N*,*N*-dimethyl-4-aminopyridine (DMAP) in 1 mL of MeCN was slowly added to a solution of 40 mg (0.050 mmol) of **1** in 5 mL of MeCN. The dark-green solution, thus obtained, did *not* require the addition of silver tetrafluoroborate ($AgBF_4$) to isolate the DMAP adduct. An addition of 10 mL of degassed Et_2O and a slow cooling at −40 °C afforded dark-green microcrystals of the desired product in 72% yield. Anal. calcd for $C_{35}H_{40}Cl_2FeN_5O_2S_2$: C 55.78, H 5.35, N 9.29; found: C 55.53, H 5.68, N 9.12. IR bands (KBr matrix, cm^{-1}): 1 614 (vs, $\nu_{CN/DMAP}$), 1 590 (vs, ν_{CO}), 1 535 (s), 1 456 (vs), 1 309 (vs), 1 225 (m), 1 009 (m), 943 (w), 745 (m). UV/vis in MeCN, λ in nm (ε in M^{-1} cm^{-1}): 475 sh (2 390), 590 (1 930). Value of μ_{eff} (298 K, polycrystal): 3.74 μ_B. EPR spectrum, frozen MeCN/toluene glass (125 K): g = 4.39, 1.98.

(Et_4N)[(Cl_2PhPepS)Fe(NO)(DMAP)] (8). Method A. A small batch of **7** (0.020 g, 0.025 mmol) was dissolved in 4 mL of degassed MeCN:Et_2O (1:3) mixture. The green solution was then cooled to −40 °C, treated with 1 equiv of NO gas in the headspace of the Schlenk flask, and stored at −40 °C for 72 h. The red crystals (suitable for diffraction studies), thus obtained, were collected by filtration, washed several times with Et_2O, and dried under vacuum. Yield: 12 mg (61%). Anal. calcd for $C_{35}H_{40}Cl_2FeN_6O_3S_2$: C 53.64, H 5.15, N 10.72; found: C 53.38, H 5.34, N 10.81. Selected IR bands (KBr matrix, cm^{-1}): 1 850 (vs, ν_{NO}), 1 625 (s, $\nu_{CN/DMAP}$), 1 583 (s, ν_{CO}), 1 529 (vs), 1 454 (vs), 1 336 (vs), 1 230 (m), 1 182 (w), 1 062 (w), 1 012 (m), 806 (w), 793 (w), 750 (m). UV/vis in MeCN, λ in nm (ε in M^{-1} cm^{-1}): 565 (2 570), 970 (1 710).

Method B. Complex **8** can be conveniently synthesized in a larger scale at room temperature by this method. A batch of **1** (200 mg, 0.262 mmol) was dissolved in 3 mL of MeCN and to it was added 150 mg (0.750 mmol) of DMAP (3 equiv). Next, 6 mL of degassed Et_2O was slowly added to the reaction mixture, and the green solution was vigorously stirred at room temperature. As the solution was stirred, a stream of dry NO(g) was allowed to bubble through it. Within several min, **8** separated out of the reaction mixture as a violet microcrystalline solid. Yield: 150 mg (65%). Since **8** cannot be recrystallized from common organic solvents (it undergoes NO dissociation), method A was required for obtaining crystals of **8** suitable for the structural studies. However, for bulk measurements (IR, reactivity studies, and in the synthesis of **9**), samples obtained via method B were used.

(Et_4N)[(Cl_2PhPep{$\underline{SO_2}$}$_2$)Fe(NO)(DMAP)] (9). A batch of **8** (180 mg, 0.23 mmol) was dissolved in 120 mL of $CHCl_3$ at −40 °C containing 84 mg (0.69 mmol) of DMAP. Next, a solution of 211 mg (0.92 mmol) of (1*S*)-(+)-(10-camphorsulfonyl)-oxaziridine in 6 mL of $CHCl_3$ was added dropwise to the red solution of **8** and DMAP, and the whole reaction mixture was slowly warmed up to room temperature. It was then stirred in the *dark* for 3 h. The resulting orange solution was filtered, and the solvent was removed under reduced pressure. Next, the residue was stirred in 2 mL of THF for 48 h at −20 °C in the dark to remove the oxaziridine reaction byproduct. The orange product, thus obtained, was collected and dried in vacuo. Yield: 170 mg (81%). The product was finally recrystallized from MeCN/Et_2O mixture at −20 °C (in the dark) to obtain red flakes. Note: **9** slowly decomposes at room temperature even under N_2 atmosphere and is quite sensitive to light. Anal. calcd for $C_{35}H_{40}Cl_2FeN_6O_7S_2$: C 49.59, H 4.77, N 9.92; found: C 50.38, H 5.02, N 9.81. Selected IR bands (KBr matrix, cm^{-1}): 1 842 (vs ν_{NO}), 1 623 (s $\nu_{CN/DMAP}$), 1 598 (s ν_{CO}), 1 457 (vs), 1 228 (s), 1 077 (m ν_{SO}), 1 042 (m ν_{SO}), 1 009 (m ν_{SO}), 791 (w), 588 (w). UV/vis in MeCN, λ in nm (ε in M^{-1} cm^{-1}): 450 (3 200). ESI-MS: m/z = 721.1. The S-oxygenated ligand was identified by mass spectral measurements on solutions of **9** in MeCN containing 0.1% trifluoroacetic acid (TFA) (m/z = 519.93).

Table 1. Summary of Crystal Data and Structure Solution Parameters for **1**·0.5Tol, **2**·2MeCN, **4**·0.5MeCN·Et_2O, **7**·THF·Et_2O·0.5MeCN, and **8**

	1	**2**	**4**	**7**	**8**
empirical formula	$C_{39.5}H_{54}N_4O_2S_2Cl_3Fe$	$C_{60}H_{66}Cl_4Fe_2N_{10}O_6S_4$	$C_{37}H_{44}Cl_2FeN_{4.50}O_{2.75}S_2$	$C_{42}H_{56.5}N_{5.5}O_{3.5}S_2Cl_2Fe$	$C_{35}H_{40}N_6O_3S_2Cl_2Fe$
formula weight	843.19	1404.97	786.64	885.30	783.60
crystal color	dark-red	violet	dichroic red/green	dichroic red/green	red shard
size, mm	0.19 × 0.14 × 0.13	0.13 × 0.05 × 0.03	0.21 × 0.19 × 0.03	0.28 × 0.24 × 0.14	
T (K)	153(2)	193(2)	153(2)	153(2)	150(2)
wavelength, Å	0.71073	0.7749	0.71073	0.71073	0.77490
crystal system	monoclinic	triclinic	triclinic	triclinic	triclinic
space group	$P2_1/c$	$P\bar{1}$	$P\bar{1}$	$P\bar{1}$	$P\bar{1}$
a, Å	13.7465(17)	10.619(2)	13.4773(12)	13.4564(14)	9.6049
b, Å	16.541(2)	12.631(3)	16.3851(15)	18.400(2)	9.6051
c, Å	19.160(2)	13.651(3)	18.9445(17)	18.930(2)	19.251
α, deg	90	66.951(4)	78.9800(10)	86.3500(10)	82.72
β, deg	109.246(2)	69.002(4)	79.4000(10)	79.8400(10)	82.65
γ, deg	90	71.607(4)	72.8100(10)	79.0150(10)	88.48
V, Å^3	4113.3(9)	1539.8(5)	3886.5(6)	4527.0(8)	1747.1(6)
Z	4	1	4	4	2
d_{calc}, g/cm^3	1.362	1.515	1.344	1.299	1.490
μ, mm^{-1}	0.702	1.058	0.673	0.588	0.944
GOF[a] on F^2	1.031	1.044	0.993	1.035	1.060
final R indices	$R1 = 0.0345$	$R1 = 0.0496$	$R1 = 0.0464$	$R1 = 0.0613$	$R1 = 0.0772$
$[I > 2\sigma(I)]$	$wR2 = 0.0772$	$wR2 = 0.1290$	$wR2 = 0.0936$	$wR2 = 0.1693$	$wR2 = 0.2046$
R indices[b]	$R1 = 0.0505$	$R1 = 0.0731$	$R1 = 0.0920$	$R1 = 0.0958$	$R1 = 0.0973$
all data[c]	$wR2 = 0.0847$	$wR2 = 0.1406$	$wR2 = 0.1110$	$wR2 = 0.1886$	$wR2 = 0.2228$

[a] GOF = $[\sum[w(F_o^2 - F_c^2)^2]/M - N)]^{1/2}$ (M = number of reflections, and N = number of parameters refined). [b] $R1 = \sum| |F_o| - |F_c| | / \sum |F_o|$. [c] $wR2 = [\sum[w(F_o^2 - F_c^2)^2]/ \sum[w(F_o^2)^2]]^{1/2}$.

Diffusion of CH_2Cl_2 into a solution of **9** and Na−triflate in MeCN at −20 °C in the dark afforded Na−**9** as a dark-red polycrystalline solid after 6−7 days. The solid was characterized by IR spectroscopy and mass spectrometry.

X-ray Data Collection and Structure Solution and Refinement. Dark-red needles of **1**·0.5 toluene were obtained via vapor diffusion of toluene into MeCN solution of the complex under inert atmosphere at ambient temperature. Violet rods of **2**·2MeCN suitable for beamline diffraction were obtained by the slow reaction of **1** in MeCN with 1 equiv of NO in the headspace (along with N_2) at 4 °C over several days. Dichroic red/green needles of **4**·0.5MeCN/Et_2O were obtained by storing a solution of **4** in MeCN:Et_2O (1:5) at −20 °C for several weeks. Green blocks of **7**·THF/Et_2O/0.5MeCN were obtained by cooling a MeCN:THF:Et_2O (1:5:10) solution of **7** at −20 °C for several weeks. Red shards of **8** were obtained by the reaction of **1** in MeCN with 1 equiv of NO gas in the headspace in the presence of 1 equiv of DMAP at −40 °C for 5 days. Diffraction data for **1**, **4**, and **7** were collected on a Bruker Apex-II instrument using MoKα radiation ($\lambda = 0.71073$ Å), and the data were corrected for absorption. Diffraction patterns for **2** and **8** were collected at beamline 11.3.1 at the Advanced Light Source at the Lawrence Berkeley National Laboratory. All structures were solved using the standard SHELXS-97 package.[21] Additional refinement details are contained in the CIF files (see Table 1 and Supporting Information). CIF files for **7** and **8** have been included in our previous communication.[22] Instrument parameters, crystal data, and data collection parameters for all the complexes are summarized in Table 1. Selected bond distances and bond angles for **1**, **2**, **4**, **7**, and **8** are listed in Table 2.

Physical Measurements. A Perkin-Elmer Spectrum-One FT-IR spectrometer was used to obtain the IR spectra. ^{1}H NMR spectra were recorded at 298 K on a Varian 500 MHz instrument. All electronic absorption spectra were obtained with a scanning Cary 50 spectrophotometer (Varian). Magnetic moment measurements were made at 298 K with a magnetic susceptibility balance from Johnson Matthey (model MSB1), and

Table 2. Selected Bond Distances (Å) and Angles (deg) for **1**, **2**, **4**, **7**, and **8**

bond distances	**1**	**2**	**4**	**7**	**8**
Fe−N1	1.9851(14)	1.989(3)	1.958(3)	1.949(3)	1.944(9)
Fe−N2	1.9484(14)	1.958(3)	1.968(3)	1.965(3)	2.007(11)
Fe−N(O)	−	1.682(3)	−	−	1.612(10)
N−O	−	1.084(4)	−	−	1.167(11)
Fe−$N_{py/DMAP}$	−	−	2.143(4)	2.108(4)	2.065(8)
Fe−S1	2.2175(5)	2.2746(10)	2.1997(13)	2.1994(11)	2.273(5)
Fe−S2	2.2293(5)	2.2841(10)	2.2154(13)	2.2065(11)	2.279(3)
Fe−Cl	2.3453(5)	−	−	−	−
Fe−N−O	−	177.1(3)	−	−	173.2(8)

X-band EPR spectra were recorded at 125 K using a Bruker 500 ELEXSYS spectrometer. Magnetic susceptibility data for **7** and **8** were collected using a Quntum Design MPMS-XL SQUID magnetometer at temperatures ranging from 2 to 300 K under an applied magnetic field of 1000 G. Data were corrected for diamagnetic contributions using Pascal's constants.

Photolysis Experiments. The quantum yield value (ϕ) of NO photorelease from **9** was obtained using a tunable Apex Illuminator (150 W xenon lamp) equipped with a Cornerstone 130 1/8 M monochromator (measured intensity of ∼10 mW/cm^2). The samples were prepared in a 10 × 10 mm anaerobic quartz cuvette setup and placed 1 cm from the light source. Ferrioxalate was used as the actinometer in between 400 and 500 nm.[23] Solutions were prepared at ∼0.5 mM to ensure sufficient absorbance (>90%) at the irradiation wavelength, and changes in electronic spectrum in the 450 nm region (<10% photolysis) were used to determine the extent of NO photorelease. For qualitative photolysis experiments, an IL 410 Illumination System from Electro-FiberOptics Corp. (halogen lamp) was used. This system was equipped with a $\lambda \geq 400$ nm cutoff filter (measured intensity = 300 mW/cm^2) to isolate visible light.

DFT Calculations. DFT calculations were carried out using the triple-ζ basis set TZP** with both p- and d-orbital polarization functions. Calculations were carried out with the aid of the

(21) Sheldrick, G. M. *Acta Crystallograph.* **1990**, *A46*, 467.
(22) Rose, M. J.; Betterley, N. M.; Mascharak, P. K. *J. Am. Chem. Soc.* **2009**, *131*, 8340–8341.
(23) Murov, S. *Handbook of Photochemistry*; Marcel Decker: New York, 1973.

Scheme 1

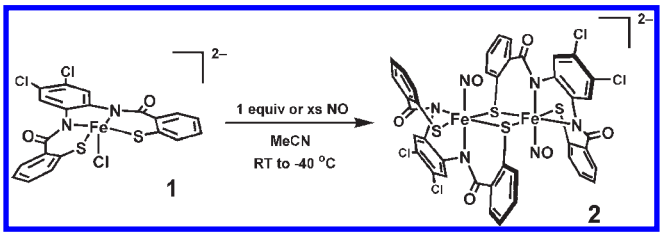

program PC-GAMESS[24] using the pure functional PW91,[25] which has been shown to be accurate for first-row transition metals and iron in particular.[26] The X-ray coordinates of **7** and **8** were used as a starting point for geometry optimization and for molecular orbital (MO) analysis. Optimized structural geometries and MOs were rendered in MacMolPlt[27] for analysis.

Results and Discussion

We have previously reported a Fe(III)−chloro complex $(Et_4N)_2[(PhPepS)Fe(Cl)]$ derived from the designed ligand $PhPepSH_4$.[28] This five-coordinate, square pyramidal species reacts with NO to afford a dimeric iron nitrosyl, namely $(Et_4N)_2[\mu\text{-}S_2\text{-}\{(PhPepS)Fe(NO)\}_2]$, in which rearrangement of the ligand frame results in bridging μ-thiolato-S donors. Based on these observations, we brought two specific changes in the synthetic strategy of the present work. First, we appended the $PhPepSH_4$ ligand frame with two chloro groups ($Cl_2PhPepSH_4$) to weaken the donor strength of the carboxamido N centers (to facilitate binding of a sixth ligand). Second, exogenous N-donor ligands (pyridine, imidazole, 4-aminopyridine, DMAP) were employed to prevent dimerization, thereby allowing isolation of a monomeric, octahedral iron nitrosyl as a synthetic model of dark-form Fe-NHase.

Metalation of the deprotonated ligand $Cl_2PhPepS^{4-}$ (using NaH as base) with $(Et_4N)[FeCl_4]$ in DMF proceeded smoothly to afford the chloro-adduct $(Et_4N)_2[(Cl_2PhPepS)Fe(Cl)]$ (**1**). Reaction of the red solutions of **1** in MeCN with NO at temperatures between room temperature and −40 °C, however, led only to isolation of the violet dimeric species $(NEt_4)_2[\mu\text{-}S_2\text{-}\{(Cl_2PhPepS)Fe(NO)\}_2]$ (**2**, Scheme 1). It was, thus, evident that the chloro groups alone were not sufficient to enable isolation of a monomeric nitrosyl. When the reaction was performed in protic media, like a 1:1 mixture of MeCN and MeOH at −40 °C, reductive nitrosylation[29] led to the formation of the corresponding $\{Fe-NO\}^7$ species $(Et_4N)_2[(Cl_2PhPepS)Fe(NO)]$ (**3**). At a higher temperature (such as room temperature), the reaction led to decomposition.

Scheme 2

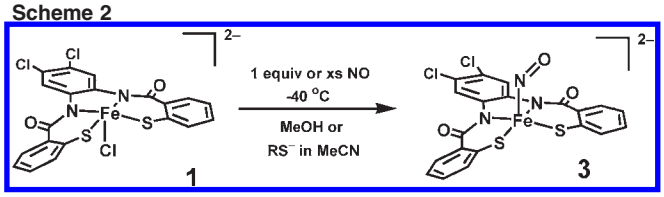

Scheme 3

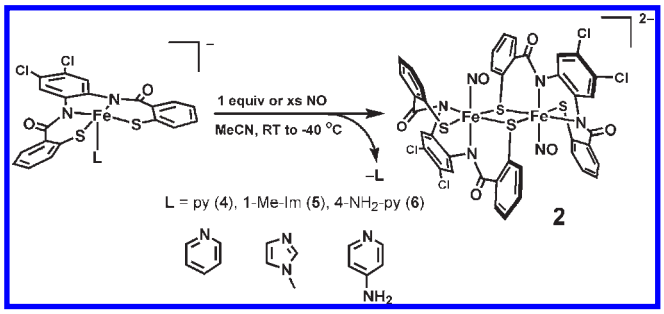

With the goal of isolation of a iron nitrosyl with N2S3 donor set (as found in $Fe\text{-}NHase_{dark}$), we also attempted reactions of **1** with NO in the presence of thiolates, such as $4\text{-}Cl-C_6H_4S^-$, $4\text{-}CF_3-C_6H_4S^-$, or $4\text{-}NO_2-C_6H_4S^-$ (as Na or Et_4N salts). Once again, these reactions afforded only the reduced $\{Fe\text{-}NO\}^7$ species with no bound thiolate (Scheme 2).

Reactions of **1** with NO in MeCN in the presence of other neutral N-donors, such as pyridine (py; $pK_a \approx 5$), 1-Me−imidazole (Me−Im; $pK_a \approx 7$), $4\text{-}NH_2$−pyridine (4AP; $pK_a \approx 8$), and *N*,*N*-4-dimethylaminopyridine (DMAP; $pK_a \approx 10$) afforded mixed results. In case of the first three N-donors (Scheme 3), the red solution of **1** in MeCN turned to deep green, indicating the displacement of Cl^- by the N-donor. However, when the green solution of $(Et_4N)[(Cl_2PhPepS)Fe(py)]$ (**4**) was treated with 1 equiv of NO(g), the violet dimeric species **2** was obtained. The strong trans effect of NO is presumably responsible for the forced displacement of the N-donors and the eventual dimerization in all these reactions.

The reaction with DMAP led to a very different result. With this N-donor of increased donor strength, the initial green complex $(Et_4N)[(Cl_2PhPepS)Fe(DMAP)]$ (**7**) reacted with NO(g) to form a pale-red solution from which the desired six-coordinate iron nitrosyl $(Et_4N)[(Cl_2PhPePS)Fe(NO)(DMAP)]$ (**8**) was isolated in good yield (Scheme 4).

It is noteworthy to mention here that in the case of $(Et_4N)_2[(PhPepS)Fe(Cl)]$, derived from the previously reported ligand $PhPepSH_4$, the reaction with NO in the presence of DMAP led only to decomposition of the reaction mixture (even at −40 °C). It is, therefore, evident that both the presence of DMAP and the chloro groups on the ligand frame are required for the isolation of a monomeric $\{Fe\text{-}NO\}^6$ nitrosyl with this type of ligand with carboxamido-N and thiolato-S donors.

Isolation of a S-oxygenated complex, to more accurately model the ligation sphere of Fe-NHase, faces several synthetic challenges. Iron nitrosyls derived from thiolate ligands are, in general, prone to decomposition via disulfide formation, NO oxidation (NO_2, N_2O_3 formation), or oxidation at the metal center. We have previously reported oxygenation of

(24) (a) Granovsky, A. A. *PC GAMESS version 7.1.5*, Gordon Research Group: Iowa State University, Ames, IA; http://classic.chem.msu.su/gran/gamess/index.html. (b) Nemukhin, A. V.; Grigorenko, B. L.; Granovsky, A. A. *Moscow Univ. Chem. Bull.* **2004**, *45*, 75.

(25) (a) Perdew, J. P.; Chevary, J. A.; Vosko, S. H.; Jackson, K. A.; Pederson, M.; R.; Singh, D. J.; Fiolhais, C. *Phys. Rev. B: Condens. Matter* **1993**, *48*, 4978. (b) Perdew, J. P.; Chevary, J. A.; Vosko, S. H.; Jackson, K. A.; Pederson, M. R.; Singh, D. J.; Fiolhais, C. *Phys. Rev. B: Condens. Matter* **1992**, *46*, 6671–6687.

(26) (a) Panchmatia, P. M.; Sanyal, B.; Oppeneer, P. M. *Chem. Phys.* **2008**, *343*, 47–60. (b) Tong, G. S. M.; Wong, E. L. M.; Che, C.-M. *Chem.—Eur. J.* **2008**, *14*, 5495–5506. (c) Conradie, J.; Quarless, D. A., Jr.; Hsu, H.-F.; Harrop, T. C.; Lippard, S. J.; Koch, S. A.; Ghosh, A. *J. Am. Chem. Soc.* **2007**, *129*, 10446–10456. (d) Han, W. G.; Liu, T. Q.; Lovell, T.; Noodleman, L. *J. Comput. Chem.* **2006**, *27*, 1292–1306. (e) Daku, L. M. L.; Vargas, A.; Hauser, A.; Fouqueau, A.; Casida, M. E. *Chem. Phys. Chem.* **2005**, *6*, 1393–1410.

(27) Bode, B. M.; Gordon, M. S. MacMolPlt: A Graphical User Interface for GAMESS. *J. Mol. Graphics. Model.* **1998**, *16*, 133−138.

(28) Harrop, T. C.; Olmstead, M. M.; Mascharak, P. K. *Inorg. Chem.* **2005**, *44*, 6918–6920.

(29) (a) Patra, A. K.; Rose, M. J.; Olmstead, M. M.; Mascharak, P. K. *J. Am. Chem. Soc.* **2004**, *126*, 4780–4781. (b) Patra, A. K.; Rowland, J. M.; Marlin, D. S.; Eckhard, B.; Olmstead, M. M.; Mascharak, P. K. *Inorg. Chem.* **2003**, *42*, 6812–6823. (c) Gwost, D.; Caulton, K. G. *Inorg. Chem.* **1973**, *12*, 2095–2099.

Scheme 4

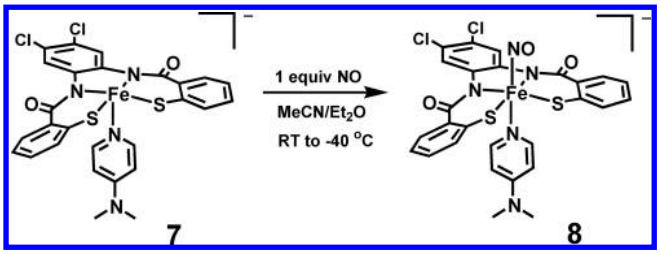

Scheme 5

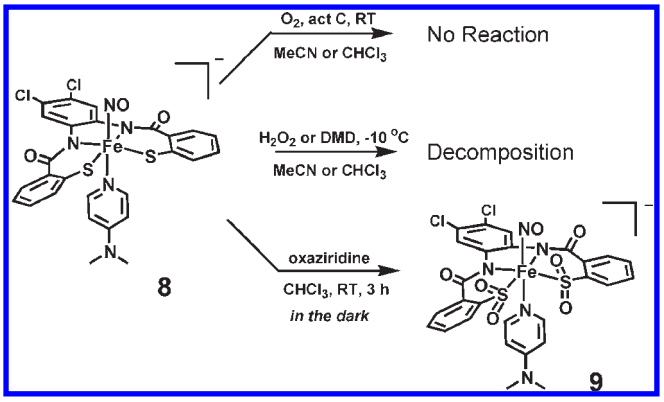

metal-bound thiolates under mild conditions.[14,16b] Surprisingly, the DMAP-bound species **7** and its nitrosyl congener **8** are *insensitive* to O_2, even upon prolonged exposure (hours) at room temperature over activated carbon (Scheme 5).[30] The use of stronger oxygenating agents, like H_2O_2[15,16a,17] and dimethyldioxirane,[18] has been reported in literature. In case of the present complex **8**, these agents were also ineffective at −40 °C and led only to decomposition of the reaction mixture at higher temperatures (≥−10 °C, Scheme 5). Since oxaziridines have been successfully used to generate sulfoxides,[31] sulfones,[32] and sulfinic acids[33] in the organic chemistry literature, we employed this oxygenation agent in our final attempt. Although (1*S*)- or (1*R*)-(+)-10-camphorsulfonyl-oxaziridine (denoted hereafter as 'oxaziridine') did not react with **8** in $CHCl_3$ at −40 °C, warming of the reaction mixture to room temperature resulted in a change of color from pale-red to orange over several hours (kept in the *dark*). Removal of the solvent in vacuo followed by THF wash afforded an orange solid. Spectroscopic analysis confirmed its formulation as $(Et_4N)[(Cl_2PhPep\{\underline{S}O_2\}_2)Fe(NO)(DMAP)]$ (**9**, Scheme 5). The presence of S-bound sulfinate donors is evidenced by strong IR stretching bands at 1077, 1042, and 1009 cm^{-1}, similar to those observed in structurally characterized Fe- and

(30) We believe that the presence of an axial thiolate ligand (in place of DMAP) could result in sensitivity to S-oxygenation by dioxygen (much like the active site of the enzyme). This has also been suggested by a reviewer of this article. However, rapid reduction of **1** upon addition of thiolate (Scheme 2) has precluded synthesis of a Fe(III) thiolate species. Further work along this line is ongoing in this laboratory at the present time.

(31) (a) Kou, H.; Kawamoto, K.; Inamoto, K.; Sakamoto, T.; Doi, T. *Tet. Lett.* **2009**, *50*, 2115–2118. (b) Davis, F. A.; Jenkins, L. A.; Billmers, R. L. *J. Org. Chem.* **1986**, *51*, 1033–1040.

(32) (a) Sandrinelli, F.; Perrio, S.; Baslin, P. *Org. Lett.* **1999**, *1*, 1177–1180. (b) Davis, F. A.; Towson, J. C.; Weismiller, M. C.; Lal, S.; Carrol, P. J. *J. Am. Chem. Soc.* **1988**, *110*, 8477–8482.

(33) (a) Martin, C.; Sandrinelli, F.; Perrio, C.; Perrio, S.; Lasne, M.-C. *J. Org. Chem.* **2006**, *71*, 210–214. (b) Okazaki, R.; Goto, K. *Heteratom Chem.* **2002**, *13*, 414–418.

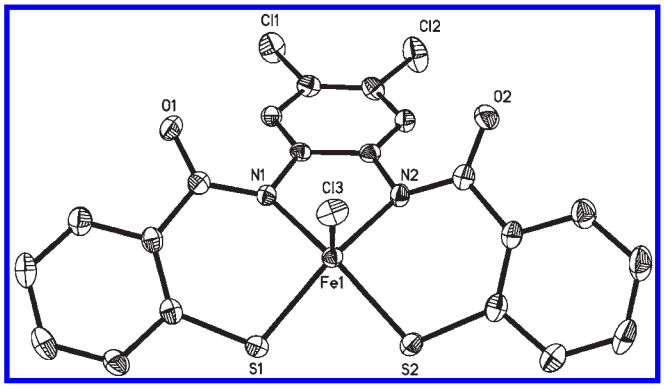

Figure 1. Thermal ellipsoid plot (50% probability level) of $[(Cl_2PhPepS)Fe(Cl)]^{2-}$, anion of **1**. Hydrogen (H)-atoms are omitted for clarity.

Co-sulfinato species.[17,34] This complex is stable in $CHCl_3$ or MeCN for days at low temperatures (≤−40 °C). The successful isolation of **9** allowed us to explore the electronic properties and the NO photolability of a model of Fe-NHase (dark form) for the first time. The results are described in the following sections.

Structures of the Complexes. $(Et_4N)_2[(Cl_2PhPepS)Fe(Cl)]$ (1). The X-ray structure of the chloro-adduct **1** (Figure 1) reveals a square pyramidal geometry around the iron center with the tetradentate $Cl_2PhPepS^{4-}$ ligand occupying the four equatorial positions and with the Cl^- ion in the axial site. The metric parameters of **1** are very similar to those of $(Et_4N)_2[(PhPepS)Fe(Cl)]$.[28] For example, the Fe−S (2.212(3), 2.219(3) Å) and Fe−Cl (2.347(3) Å) bond distances of **1** are very close to the corresponding distances noted for $(Et_4N)_2[(PhPepS)Fe(Cl)]$ (Fe−S = 2.2102(7); Fe−Cl = 2.3471(6) Å). Also, the diaminobenzene moiety of the ligand is tilted downward by approximately 30° from the equatorial plane defined by the N2S2 donor set.

$(Et_4N)_2[\mu\text{-}S_2\text{-}\{(Cl_2PhPepS)Fe(NO)\}_2]$ (2). The structure of the dimeric nitrosyl **2** is shown in Figure 2. The overall structure of **2** resembles that of $(Et_4N)_2[\mu\text{-}S_2\text{-}\{(PhPepS)Fe(NO)\}_2]$,[28] reported by us previously. In both cases, the ligand is rearranged such that the carboxamido-N is trans to the apical NO, and one thiolato-S from each ligand acts as a bridging atom between the two metal centers. The carboxamido-N trans to NO lies further away from the metal center (Fe−N1 = 1.989(3) Å) compared to that of the equatorial carboxamido-N donor (Fe−N2 = 1.958(3) Å), most possibly due to the trans effect of NO.

$(Et_4N)[(Cl_2PhPepS)Fe(py)]$ (4). Substitution of Cl^- for py affords the pyridine congener **4** from **1**. Despite the use of excess pyridine, the reaction affords **4** whose structure shows only one py bound to the metal center (Figure 3). As shown in Table 2, the Fe−N and Fe−S bond distances of **4** are quite similar to those observed in the chloro-adduct **1**. The Fe−N_{py} distance (2.144(4) Å) is shorter than that of the corresponding Fe−Cl distance in **1** (2.347(3) Å). The Fe−N(carboxamido) bond distances (1.958(3), 1.968(3) Å) of **4** are noticeably shorter than the Fe−N_{py} distance, presumably due to the much stronger σ-donor strength of the deprotonated carboxamido-N versus the neutral pyridine-N donor.

(34) Yano, T.; Arii, H.; Yamaguchi, S.; Funahashi, Y.; Jitsukawa, K.; Ozawa, T.; Masuda, H. *Eur. J. Inorg. Chem.* **2006**, 3753–3761.

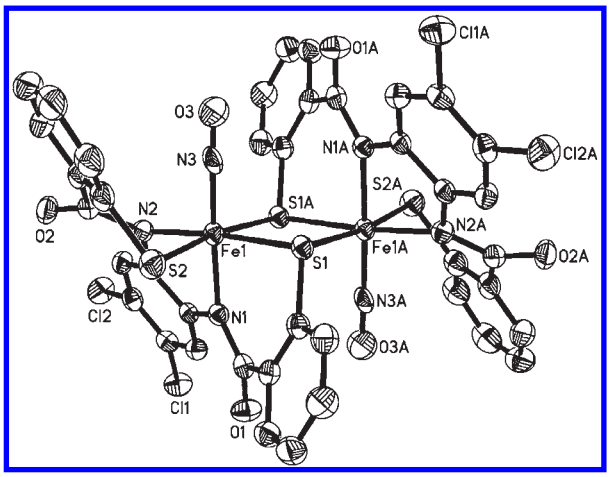

Figure 2. Thermal ellipsoid plot (50% probability level) of $[\mu\text{-}S_2\text{-}\{(Cl_2\text{-}PhPepS)Fe(Cl)\}_2]^{2-}$, anion of **2**. H-atoms are omitted for clarity.

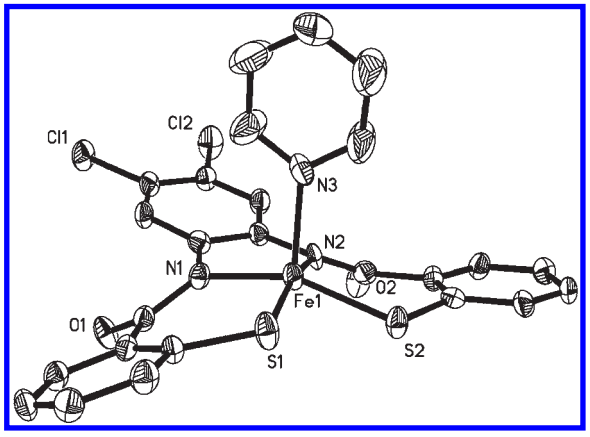

Figure 3. Thermal ellipsoid plot (50% probability level) of $[(Cl_2PhPepS)Fe(py)]^-$, anion of **4**. H-atoms are omitted for clarity.

(Et_4N)[(Cl_2PhPepS)Fe(DMAP)] (7). The DMAP-bound species **7** bears much structural resemblance to pyridine-adduct **4**, both in terms of its overall square pyramidal geometry (Figure 4) and its bond distances (Table 2). The only difference is the Fe−N_{DMAP} bond distance (2.108(4) Å), which is slightly shorter than the corresponding Fe−N_{py} bond length (2.144(4) Å) noted in **4**, again due to the greater σ-donor strength of N_{DMAP} versus N_{py}.

(Et_4N)[(Cl_2PhPepS)Fe(NO)(DMAP)] (8). The structure of **8**, shown in Figure 5, resembles that of **7** with additional coordination of NO at the sixth position. In this monomeric nitrosyl, the iron center lies in a pseudo-octahedral geometry with NO coordinated trans to DMAP. The Fe−N(carboxamido) bond distances are slightly asymmetric in this structure (Fe−N1 = 1.944(9); Fe−N2 = 2.007(11) Å), owing to the differing distortion angles of the benzene−thiolate moieties on each side of the ligand frame. A change in the spin state of the iron center (vide infra) makes the Fe−N_{DMAP} bond distance of **8** (2.065(8) Å) shorter than the corresponding distance in **7** (Fe−N_{DMAP} = 2.108(4) Å). The Fe−N(O) distance (1.612(1) Å) in monomeric **8** is shorter than the corresponding Fe−N(O) bond length in the dimeric nitrosyl **2** (1.682(3) Å), while the N−O bond distance (1.167(11) Å) is longer than that observed in **2** (1.084(4) Å).

NO Photolability. Addition of 1 equiv of NO to a green solution of **7** in MeCN at −20 °C rapidly affords a red

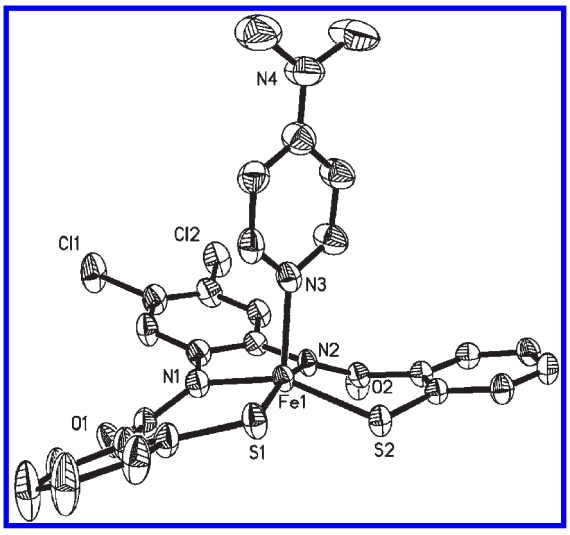

Figure 4. Thermal ellipsoid plot (50% probability level) of $[(Cl_2PhPepS)Fe(DMAP)]^-$, anion of **7**. H-atoms are omitted for clarity.

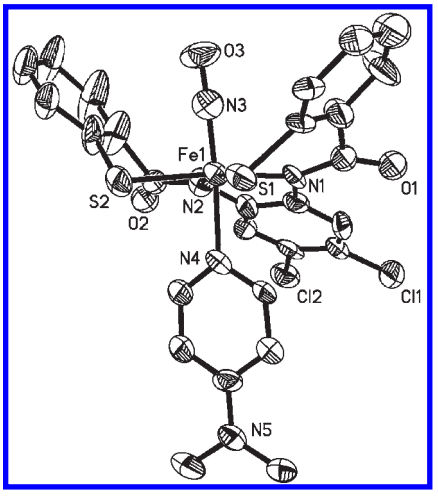

Figure 5. Thermal ellipsoid plot (50% probability level) of $[(Cl_2PhPepS)Fe(NO)(DMAP)]^-$, anion of **8**. H-atoms are omitted for clarity.

solution of **8** (Figure 6). When the red solution is placed under vacuum, the green color of **7** is regenerated within seconds. This cycle of NO addition and release (under vacuum) can be repeated several times with minimal decomposition of the reaction mixture (Figure 6).[35] Surprisingly, **8** *does not* exhibit any NO photolability; exposure of solutions of **8** in MeCN to UV or visible light does not result in the release of NO. Collectively, these results demonstrate that the bound NO in **8** is thermally labile but is insensitive to light. Quite in contrast to the behavior of **8**, the S-oxygenated nitrosyl **9** rapidly releases NO when exposed to low-power visible light ($\lambda \geq 400$ nm, 300 mW/cm^2).[22] Exposure of a solution of **9** in MeCN (or $CHCl_3$) at 0 °C to low-power visible light (10 mW/cm^2) results in a rapid release of NO (as detected by a NO-sensitive electrode, Figure 7) and a change in color from orange to pale-green. This behavior resembles that of Fe-NHase quite closely. IR measurements on the irradiated

(35) Similar behavior of bound NO has been noted in $\{Fe\text{-}NO\}^6$ nitrosyls derived from porphyrin ligands; seeEllison, M. K.; Scheidt, W. R. *J. Am. Chem. Soc.* **1999**, *121*, 5210–5219.

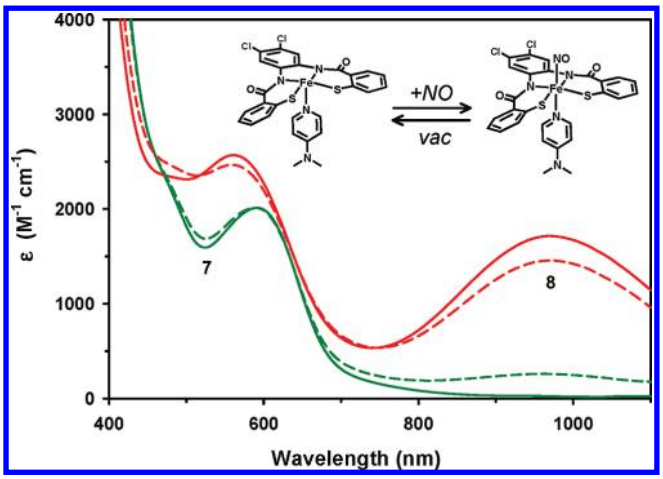

Figure 6. Electronic absorption spectra in MeCN (experiment performed at 298 K) showing reversible conversion of **7** (green traces) to **8** (red traces). Two cycles are shown.

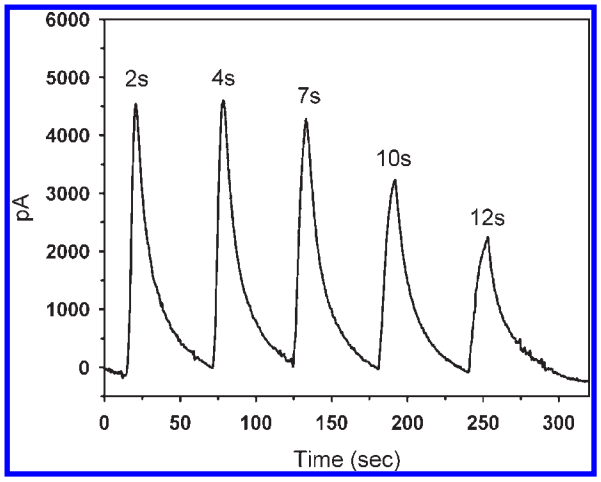

Figure 7. Amperogram generated with an *ami*NO-2000 electrode upon exposure of Na[(Cl_2PhPepSO_2)Fe(NO)(DMAP)] (**9**) in MeCN/H_2O (1:1) solution to low-intensity visible light (10 mW/cm^2) at 0 °C. The decreasing response at longer light-exposure times is due to nearly complete photolysis of the solution of **9** (~0.5 mM) after 30 s of total irradiation time.

solution also confirm loss of NO from **9** upon illumination. Quantum yield measurements (λ_{irr} = 450 nm) at room temperature have afforded a ϕ value of 0.55 for **9** in a MeCN solution (value for Fe-NHase$_{dark}$ = 0.48).[9a] EPR and mass spectral measurements on the an irradiated solution of **9** in MeCN containing 2 equiv DMAP reveal the formation of a low-spin [(Cl_2PhPep{$\underline{SO_2}$}$_2$)Fe(DMAP)$_2$]$^-$ (**10**, g = 2.23, 2.03, and 2.02; m/z = 823.1) as the photoproduct.[22] Taken together, the results demonstrate that oxygenation of the thiolato-S centers in **8** imparts NO photolability to the S-oxygenated product **9**.

NO Transfer Reactions. The ability of **7** to rapidly capture NO (via formation of **8**) prompted us to perform several NO transfer reactions. Since **8** exhibits a unique absorption band in the 1 000 nm range (Figure 6), one can easily follow the "NO capture" reaction, even in presence of other species in solution. In our first NO transfer reaction, we employed a photoactive {Mn−NO}^{6} nitrosyl namely, [($PaPy_3$)Mn(NO)]ClO_4 (denoted as Mn−NO hereafter).[36] As reported by us in a previous account, Mn−NO rapidly releases NO upon exposure to visible light (ϕ_{550} = 0.80).[37] When **7** was mixed with Mn−NO and kept in the *dark*, no change was observed even after 1 h. However, when the mixture was exposed to light (~30 s), a color change to red was observed, and the appearance of the 1 000 nm band (isosbestic points at 590, 670 nm, Figure S1, Supporting Information) confirmed the formation of **8** via transfer of NO from Mn−NO to **7** (Scheme 6).

Scheme 6. NO Transfer Reaction from the Light-Triggered NO Donor Mn−NO to the Precursor Fe(III)−DMAP Complex (**7**) Described in This Work

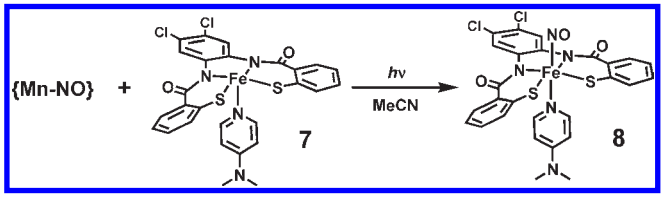

Since the S-oxygenated nitrosyl **9** is photolabile, we have also performed a NO exchange reaction between **9** and **7** (Scheme 7). When a 1:1 mixture of **7** and **9** in MeCN was kept in the *dark* for 15 min, no change in the electronic absorption spectrum was noted. Brief exposure of this mixture to light ($\lambda \geq$ 400 nm, 300 mW/cm^2), however, rapidly led to the formation of **8** (color changed to pale red). As shown in Figure 8, the electronic spectrum of the reaction mixture shows a time- and light-dependent NO transfer from complex **9** to **7**. Isosbestic points at 580, 650 nm indicate clean NO transfer from **9** to **7** (Scheme 7) in this reaction under illumination.

DFT Calculations. In order to gain insight into the reason(s) behind the different NO photoreactivity of the two nitrosyls **8** and **9**, we have performed DFT calculations on selected complexes. The DFT optimized geometries of **7**, **8**, and **9** are shown in Figure 9 for comparison, and the details of the calculations on each complex are given below.

Calculations on the various possible spin states of the Fe(III)−DMAP species **7** indicated that the lowest-energy spin configuration would be S = 3/2 (Figure S2, Supporting Information). This is in agreement with the experimental EPR spectrum (g = 4.39, 1.98 broad signal), with the room temperature magnetic moment value (μ_{eff} = 3.87 μ_B), and with the results of the temperature-dependent magnetic susceptibility measurements (Figure 10). As shown in Table 3, geometry optimization on the coordinates of **7** (S = 3/2 state) reveals high structural similarity to its crystal structure in terms of Fe−S and Fe−N bond distances. The only exception is the slightly elongated Fe−N_{DMAP} bond distance predicted by DFT (2.19 Å), as compared to the somewhat shorter Fe−N_{DMAP} distance found in the crystal structure (2.108(4) Å). The highest occupied molecular orbital (HOMO) through HOMO−3 orbitals of **7** are dominated by carboxamido-N and thiolato-S orbitals (Figure S3,

(36) Ghosh, K.; Eroy-Reveles, A. A.; Avila, B.; Holman, T. R.; Olmstead, M. M.; Mascharak, P. K. *Inorg. Chem.* **2004**, *43*, 2988–2997.

(37) (a) Eroy-Reveles, A. A.; Leung, Y.; Beavers, C. M.; Olmstead, M. M.; Mascharak, P. K. *J. Am. Chem. Soc.* **2008**, *130*, 4447–4458. (b) Eroy-Reveles, A. A.; Leung, Y.; Mascharak, P. K. *J. Am. Chem. Soc.* **2006**, *128*, 7166–7167.

Scheme 7. NO Transfer from the Light-Sensitive Iron Nitrosyl **9** to **7** upon Brief Exposure to Visible Light[a]

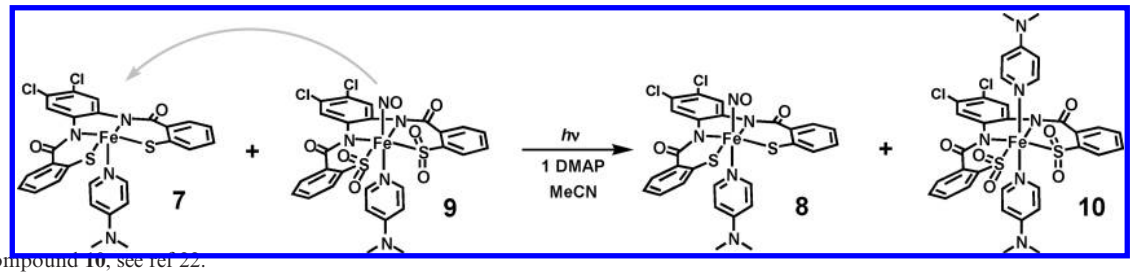

[a] For Compound **10**, see ref 22.

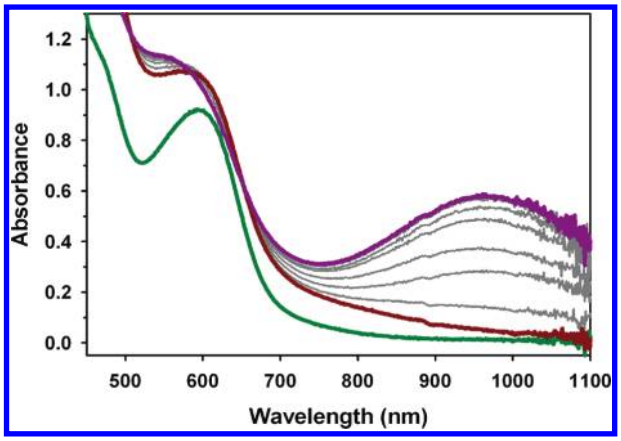

Figure 8. Electronic absorption spectra (in MeCN) demonstrating NO transfer from **9** to **7**; complex **7** alone (dark-green line); **7** plus **9** (dark-red line); light-dependent NO transfer (5−40 s light pulses) resulting in formation of **8** (violet line). The new peak generated at ∼1 000 nm indicates the formation of **8**.

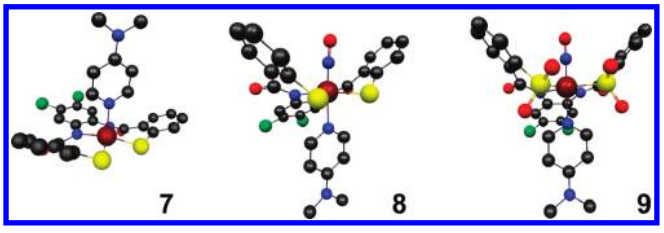

Figure 9. DFT calculated and geometry-optimized (PW91/TZP** DFT basis set) structures of complexes **7**, **8**, and **9**. H-atoms are omitted for clarity.

Supporting Information), while the Fe-based singly occupied molecular orbitals (SOMOs) reside at slightly lower energies.

In case of the nitrosyl **8**, DFT calculations predicted a $S = 0$ state as the lowest energy configuration (Figure S4, Supporting Information), and a temperature-dependent magnetic susceptibility measurement (4−300 K) confirmed this configuration in the solid state. Geometry optimization afforded metric parameters that closely matched the parameters obtained from X-ray studies (Figures 5 and 9, Table 3). As shown in the left panel of Figure 11, the HOMO of **8** is indicative of mostly Fe−S bonding interactions, while HOMO−1 is dominated by interactions between the nonbonding S lone pairs and the aromatic ring systems. The HOMO−2 of **8** is interesting since it represents a three-center S−Fe−N(O) bonding scheme. In this case, the strong negative charge of the thiolato-S traverses the Fe center and continues into the Fe−N(O) bond. This S−Fe−N(O) bonding results from

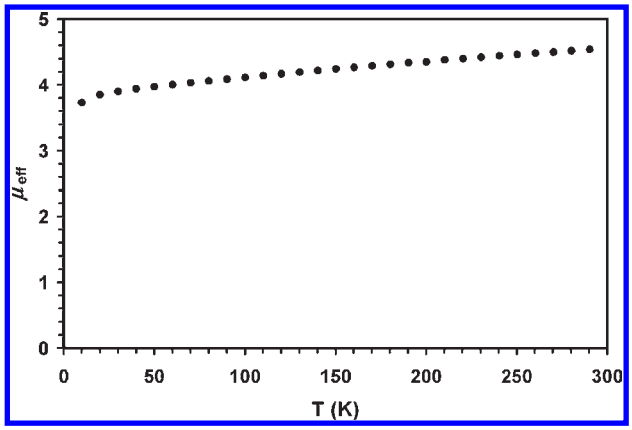

Figure 10. Plot of the temperature-dependent magnetic moment (μ_{eff}) for **7**.

Table 3. Selected Comparisons of Experimental and Calculated Bond Distances (Å) and Bond Angles (deg) for the Anions of **7**, **8**, and **9**[a]

	experimental	calculated
	$[(Cl_2PhPepS)Fe(DMAP)]^-$ (**7**)	
Fe−N1	1.949(3)	1.983
Fe−N2	1.965(3)	1.963
$Fe-N_{DMAP}$	2.108(4)	2.199
Fe−S1	2.1994(11)	2.242
Fe−S2	2.2065(11)	2.239
	$[(Cl_2PhPepS)Fe(NO)(DMAP)]^-$ (**8**)	
Fe−N1	1.944(9)	1.982
Fe−N2	2.007(11)	1.978
Fe−N(O)	1.612(10)	1.618
N−O	1.167(11)	1.160
$Fe-N_{DMAP}$	2.065(8)	2.113
Fe−S1	2.273(5)	2.329
Fe−S2	2.279(3)	2.314
Fe−N−O angle	173.2(8)°	176.0°
	$[(Cl_2PhPep\{SO_2\}_2)Fe(NO)(DMAP)]^-$ (**9**)	
Fe−N1	−	2.0178
Fe−N2	−	2.0131
Fe−N(O)	−	1.6348
N−O	−	1.1599
$Fe-N_{DMAP}$	−	2.1130
Fe−S1	−	2.3756
Fe−S2	−	2.3650
Fe−N−O angle	−	177.5°

[a] Calculated using a triple-ζ** quality DFT basis set; PW91 functional.

the strong σ- and π-donation by the thiolato-S donors coupled with the π-accepting capacity of the bound NO. This has important implications when compared to the

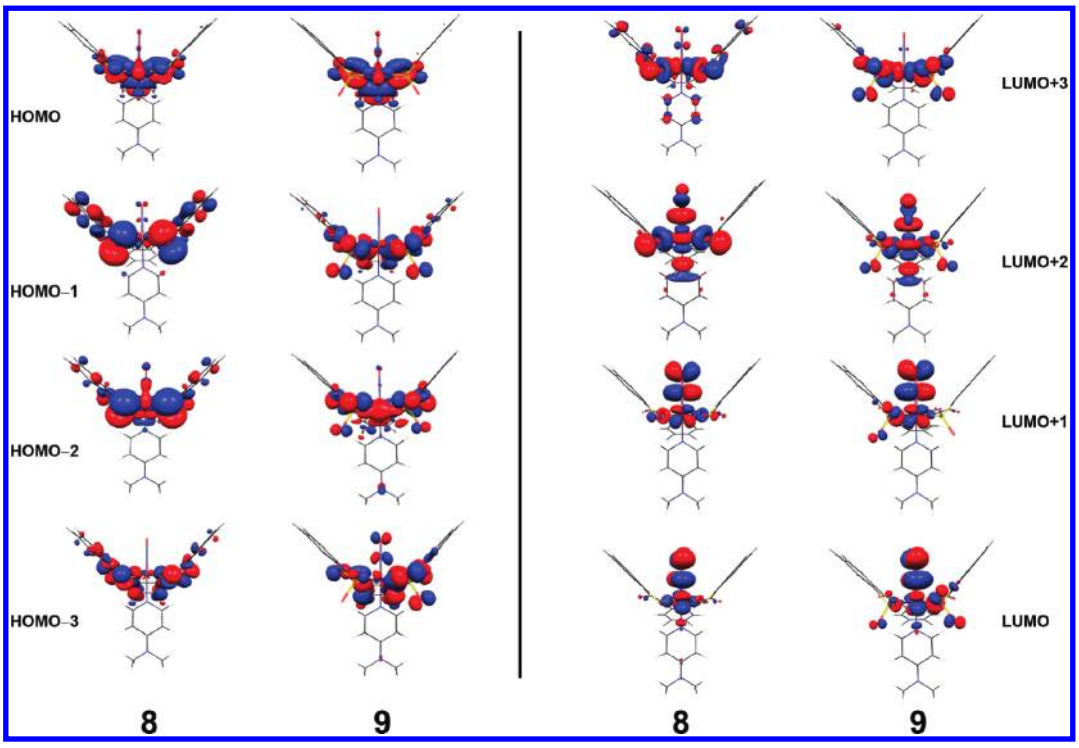

Figure 11. Left panel: DFT-calculated HOMO through HOMO−3 orbitals (from top to bottom) of **8** and of the S-oxygenated species **9**. Right panel: DFT-calculated LUMO through LUMO+3 orbitals (from bottom to top) of **8** and **9**.

Fe−SO_2 system present in **9** (vide infra). Overall, this strong S−Fe−N(O) bonding may explain the lack of NO photolability observed experimentally with **8** despite the fact that the lowest unoccupied molecular orbital (LUMO) and LUMO+1 of **8** are dominated by clear d_π(Fe)−π*(NO) antibonding interaction (right panel, Figure 11).

Time-dependent DFT (TD-DFT) calculations of the electronic absorption spectrum of **8** predict a strong visible band near ∼550 nm, as observed in the experimental spectrum (Figure 12, bottom panel). This band has its origin in the charge transfer from the thiolato-S donors to the unoccupied d_z2(Fe−NO) orbital and is denoted as p(S) → d_z2(Fe). On the other hand, the strong band observed in the experimental spectrum near 1 000 nm at room temperature is not predicted by the $S = 0$ TD-DFT calculation. Only a cluster of very weak intensity bands ($\varepsilon_{calc} < \sim 100$ M^{-1} cm^{-1}) appears in the calculated spectrum, comprising mostly of p(S) → π*(NO) transitions. Over the course of our investigations, we noted that at a low temperature (−40 °C), the intensity of the 1 000 nm absorption band of **8** is greatly diminished (Figure 12, top panel). As shown in Figure 12, the electronic spectrum of **8** at −40 °C is more similar to that of the predicted $S = 0$ TD-DFT spectrum. We have, therefore, calculated the next higher $S = 1$ spin state of **8** to check the possibility of contribution from the excited state(s). Indeed, we found two excited states with excitation energies near 1 000 nm (1 084 and 1 047 nm), correlating with the 298 K absorption spectrum of **8** (Figure 12, bottom panel). Further magnetic susceptibility studies and theoretical work are, however, required for proper identification of excited state contribution to the room temperature spectrum of **8**.

We have also constructed a structural model of the S-oxygenated nitrosyl [(Cl_2PhPep{SO_2}$_2$)Fe(NO)(DMAP)]$^-$

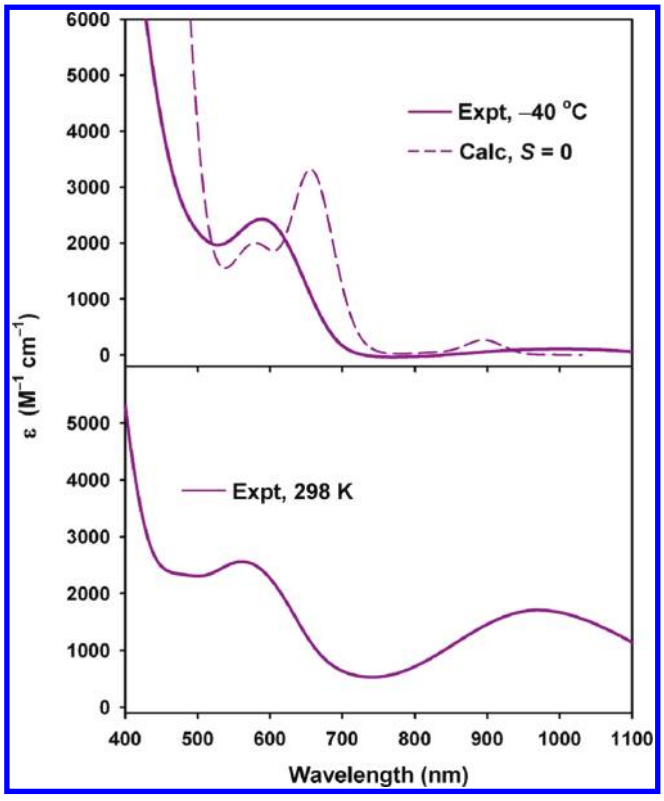

Figure 12. Top Panel: DFT-calculated (PW91/TZP**; dashed line) and low-temperature (−40 °C, solid line) experimental electronic absorption spectra of **8**. Bottom Panel: Ambient temperature electronic absorption spectrum of **8**.

(**9**) via DFT geometry optimization (Figure 9). Like **8**, spin-state calculations on **9** suggest an $S = 0$ ground state (Figure S5, Supporting Information). The largest

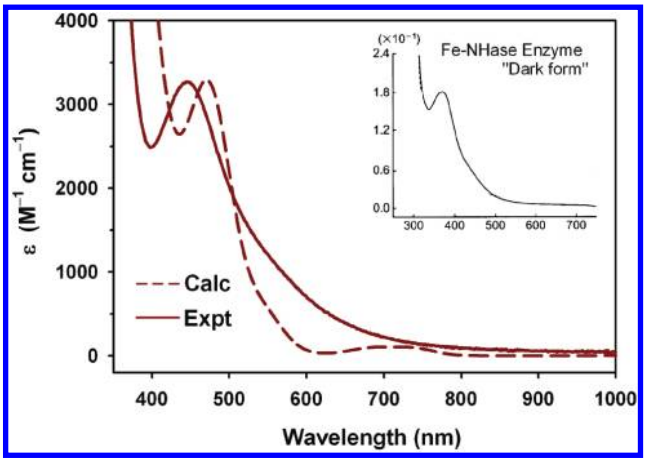

Figure 13. DFT-calculated (PW91/TZP**; dashed line) and experimental (298 K; solid line) electronic absorption spectra of **9**. Inset: Absorption spectrum of the dark form of Fe-NHase.

structural change upon S-oxygenation is the elongation of the Fe−S(O_2) bonds in **9** (calculated: 2.365 and 2.375 Å) versus the Fe−S bonds found in **8** (calculated: 2.329 and 2.314 Å; experimental: 2.273(5) and 2.279(3) Å). Such elongation arises most likely from weaker donor capacities of the sulfinate moieties (S-oxygenation lowering the donor ability of the thiolato-S centers). Additionally, S-oxygenation abolishes the π-donor capacity of the thiolato-S. The most notable change upon S-oxygenation is observed in the HOMO−2 of **9** (Figure 11, right panel). The three-center S−Fe−N(O) bonding orbital of **8** is now absent since the lone pairs on S are now involved in S−O bonding. As a consequence, the Fe−N(O) bond is weakened significantly. The LUMOs of **9**, on the other hand, remained almost unchanged (compared to **8**) and are dominated by typical d_π(Fe)−π^*(NO) antibonding interaction.

The calculated TD-DFT spectrum of **9** closely matches the experimental data (Figure 13). A cluster of dominant features calculated near 470 nm (expt: 450 nm) emanates from the carboxamido-N and sulfinato-SO_2 donors (denoted as N_{am}‖SO_2). In these transitions, the density is transferred to d_π(Fe)-π^*(NO) and d_z2(Fe)-σ^*(NO) antibonding interactions. The transfer of electron density to both π^* and σ^* antibonding orbitals is likely to be responsible for the high quantum yield values noted in NO photolability measurements with **9**, as both the π and σ components of the Fe−NO bond must be broken to promote NO photolability. We suggest that the NO photolability of **9** arises principally from this {N_{am}‖SO_2} → {d_π(Fe)-π^*(NO)‖d_z2-σ^*(NO) transition.

Richards and co-workers have reported DFT results on *theoretical* Fe-NHase models derived from crystallographic coordinates of the NO-bound *Rhodococcus* R312 NHase.[38] The results of the present work are in good agreement with several of their conclusions based on models with S- and SO/SO_2-bound iron centers. For example, in theoretical models, sulfur oxidation influences Fe−S bonding, and for the transition of the SO/SO_2-bound model at 380 nm, the electron is promoted into the Fe−NO antibonding orbital from a molecular orbital associated with the sulfinate ligand. Most interestingly, a similar transition in the S-bound model is associated with a transition that does not promote an electron into the Fe-NO antibonding orbital.

In summary, we have synthesized a model of the NO-bound dark form of Fe-NHase, namely (Et_4N)[$(Cl_2$-PhPepS)Fe(NO)(DMAP)] (**8**), with both carboxamido-N and thiolato-S donors. Although the coordination structure of **8** resembles that of the iron site in Fe-NHase, it does not exhibit the crucial property of NO photolability much like the other NO-bound models of Fe-NHase. However, the results of the present work indicate that S-oxygenation of **8** is required to turn on the NO photolability, and the properties of (Et_4N)[$(Cl_2$PhPep-{$\underline{S}O_2$}$_2$)Fe(NO)(DMAP)] (**9**) suggest that the NO photolability observed with Fe-NHase could arise from S-oxygenation of the Cys residues in the equatorial plane. In recent years, several roles of post-translational oxidative modification of Cys-S centers of proteins in regulation of a wide variety of biological processes have been recognized.[39,40] Participation of oxygenated Cys-S centers in NO photoregulation of Fe-NHases could add to the list of such regulatory processes.

Acknowledgment. This research was supported by a grant (CHE-0553405) from the National Science Foundation (NSF). The X-ray facility at University of California Santa Cruz (UCSC) is supported by a NSF Major Research Instrumentation (MRI) grant CHE-0521569. Crystallographic data for **2** and **8** were collected at the Advanced Light Source (ALS), Lawrence Berkeley National Laboratory. The ALS is supported by the United States Department of Energy Sciences under the contract DE-AC02-05CH11231. We thank Professor Jeff Long and Joe Zadrony for assistance with the temperature-dependent magnetic susceptibility (SQUID) measurements.

Supporting Information Available: Electronic absorption spectra during NO transfer from Mn−NO to **7** in MeCN (Figure S1), DFT-calculated spin-state energy diagrams for **7** (Figure S2), **8** (Figure S4), and **9** (Figure S5), extended HOMO−SOMO−LUMO diagram for **7** (Figure S3), optimized geometry coordinates, internuclear distances, and energy gradient parameters for **7**, **8**, and **9** (Tables S1−3), and X-ray crystallographic data (in CIF format) for **1**·0.5Toluene, **2**·2MeCN, and **4**·0.5MeCN·Et_2O. This material is available free of charge via the Internet at http://pubs.acs.org.

(38) Greene, S. N.; Chang, C. H.; Richards, N. G. J. *Chem. Commun.* **2002**, 2386–2387.

(39) (a) Reddie, K. G.; Carroll, K. S. *Curr. Opin. Chem. Biol.* **2008**, *12*, 746–754. (b) Poole, L. B.; Nelson, K. J. *Curr. Opin. Chem. Biol.* **2008**, *12*, 18–24.

(40) (a) D'Autreax, B.; Toledano, M. B. *Nat. Rev. Mol. Cell Biol.* **2007**, *8*, 813–824. (b) Ilbert, M.; Horst, J.; Ahrens, S.; Winters, J.; Graf, P. C.; Lilie, H.; Jakob, U. *Nat. Struct. Mol. Biol.* **2007**, *14*, 556–563.